Two-Dimensional Mapping of the Microwave Potential on MMIC's Using Electrooptic Sampling

Dag Roar Hjelme, Michael John Yadlowsky, and Alan Rolf Mickelson

Abstract— **An accurate technique for mapping the two-dimensional microwave potential in microwave circuits has been developed and tested. Using the direct electrooptic sampling technique and a de-embedding algorithm to remove substrate variation induced measurement errors, accurate two-dimensional potential maps with a dynamic range of 50 dB and spatial resolution of 10 μm are obtained. De-embedding of the microwave potential from the measured, electrooptically modulated signal is achieved by deducing the substrate parameters from the measured average reflected optical power. Once the substrate is characterized, the microwave potential can be calculated from the electrooptic signal. The de-embedding procedure technique was successfully tested on a through-line and an open-end line of a TRL microstrip calibration standard.**

I. Introduction

TWO-DIMENSIONAL (2D) maps of the microwave fields within a circuit can provide a powerful tool for studying the fundamental properties of wave propagation in various high-speed devices and circuits. For example, a 2D field distribution can provide significant insight into the process of scattering off transmission line discontinuities, the operation of active devices, and the distribution of energy in resonant structures. Furthermore, 2D field maps could be extremely useful as a diagnostic tool for testing and fault detection on large circuits, since these maps contain information that is not readily obtained from terminal characteristics.

The exact solution of Maxwell's equation for the field distribution near a transmission line discontinuity is very difficult. Nevertheless, it is this local field distribution that is needed to understand the scattering properties of the fundamental propagation mode at a discontinuity, and therefore the scattering matrix of a junction. A measurement of the 2D field distributions would provide a better understanding of the scattering process and make it possible to validate numerical models. In multimoded waveguides or cavities with complicated geometries, the solution of Maxwell's equation can be even more difficult. Until recently, the eigenmodes of these structures have been inaccessible to experiments, and consequently there has been no direct experimental validation of numerical solutions. Additionally, in active devices (as in passive devices), many of the transient physical processes determining the device characteristics manifest themselves as rapid variation of the electric field over an extended region. New insight into the device performance could be obtained by measuring the space/time dependence of the electric field in the vicinity of the device.

Early attempts to measure the electric field in open waveguides relied on various modifications of a coaxial probe. Most of this early work was concerned with measuring standing waves (1D field distributions). Measurements using a probe traveling above the strip conductor of a microstrip [1], a probe in the microstrip ground plane [2], and a coaxial probe running above a dielectric image line [3] have been reported. Due to the mechanical nature of these probes, the accuracy and spatial resolution of these techniques were quite limited. Recently, a magnetic field probe suitable for high-frequency measurements has been reported [4], [5]. However, being a mechanical probe (although noncontact), its spatial resolution was limited to several tens of micrometers, therefore making accurate nearfield measurements on monolithic microwave integrated circuits (MMIC's) difficult.

Recently, two-dimensional mapping techniques of microwave fields has been reported by a number of groups. Sridhar [6] used a cavity perturbation technique to study the eigenmodes in chaotic microwave cavities, and McCall *et al.* [7] probed through an array of small holes in a waveguide to get a spatial mapping of the electric field within a dielectric lattice. Stearns [8] measured two-dimensional spatial maps of high-voltage pulses inside vacuum waveguides with an electrooptic sampling technique that employed a small (0.8 mm on the side) $LiTaO_3$ crystal probe. By moving the probe crystal with respect to the waveguide, a 2D map of the voltage was obtained with a 0.25 mm resolution which was determined by the probe beam diameter. Kingsley *et al.* [9], [10] combined electrooptic sampling with imaging technology to study the fields in high-power photoconductive switches. Using an $LiTaO_3$ crystal on top of the photoconductive switch, and synchronizing the sampling laser system to the 30 Hz video rate of the CID camera detector, they could map spatial variations of the field without requiring translation of the sampling point across the crystal. However, the technique was limited by its low sensitivity (200 V/cm) and low repetition rate (30 Hz). Furthermore, such crystal probes are intrusive because an external crystal with very high microwave dielectric constant ($\epsilon \sim 40$) in close contact with the surface perturbs the fields.

Other techniques, including E-beam [11] and photoemissive probing [12], have been developed for logic circuits. These techniques make it possible to measure the voltage

Manuscript received June 9, 1992; revised October 20, 1992. This work was supported by the NSF Industry/University Cooperative Research Center for Microwave/Millimeter Wave Computer Aided Design under Grant CDR-8722832, and by the Office of naval Research under Grant ONRN00014-92-1190.

The authors are with the Department of Electrical and Computer Engineering, University of Colorado, Boulder, CO 80309-0425.

IEEE Log Number 9209347.

distribution on conductors with excellent spatial resolution. Two-dimensional logic-state mappings with a sensitivity of 0.2 V have been demonstrated. A "time-resolved optical beam induced current method" has also been used for 2D logic-state maps [13]. However, for accurate nearfield mapping in MMIC's, these techniques cannot easily compete with the electrooptic probing technique because of their limited dynamic range.

In this paper, we will describe how the direct electrooptic sampling technique can be used for two-dimensional microwave potential mapping on MMIC's. The direct electrooptic probing technique [14] uses the electrooptic properties of a circuit substrate to serve as a probing mechanism. This is ideal for two-dimensional mapping in planar circuits, since the probe is fully distributed. However, unlike most measurement techniques, the piece to be measured (over which one has least control) is the sensor, and unless the probing pulse is much shorter than the transit time through the substrate, substrate nonuniformities will strongly affect the accuracy of the field measurements [15]. Therefore, to be useful in applications where a comparison between different spatial points is necessary, a de-embedding technique is needed. Recently, we developed a technique for de-embedding these measurement variations from the electrooptic measurements, thereby opening the possibility of calibrated optical probing measurements [15]. Extending this technique to two-dimensional measurements, accurate field measurements with good spatial resolution become possible. In this paper, we will present a de-embedding procedure based on our earlier model of the direct electrooptic probing system [15]. In addition to the parameters in that model, the substrate front and backside reflectivities and substrate optical roundtrip phase, we extend the model to include surface roughness by accounting for phase variation across the probe beam. The utility of the de-embedding procedure is demonstrated by determining the two-dimensional potential distribution on GaAs microstrip circuits from electrooptic sampling measurements.

In the next section, we present the theoretical basis for the de-embedding procedure. From a Jones matrix analysis of the electrooptic sampling system, we derive the general form of the receiver signal. The optical properties of the circuit substrate are included by modeling the effect of the ground plane adhesion layer and surface roughness. Based on this model, a measurement procedure and data processing technique to accomplish the de-embedding are presented in Section II-C. In Section III, we present results of applying the proposed de-embedding procedure to electrooptic sampling measurements. The procedure is used to correct 2D potential distributions measured on microstrip calibration standards. Some possible future developments and improvements of the technique are discussed in Section IV.

II. Theory

A. The Electrooptic Sampling System

In the standard configuration for reflection-mode direct electrooptic probing considered here (Fig. 1), a polarizing beam splitter (PBS) and two retardation plates (WP) are used to prepare the polarization state of the incident probing beam and to separate out the reflected beam. In practice, a number of steering mirrors and beam samplers may also be used to deliver the probe beam to the sampling point and to illuminate and image the circuit. The Jones matrix relating the incident polarization state to the output polarization state can be written as

$$\begin{aligned} M &= M_y M_{wp1} M_{wp2} M_m M_s M_m M_{wp2} M_{wp1} M_x \\ &\equiv M_y M_o M_s M_i M_x \end{aligned} \tag{1}$$

where M_s represents the circuit substrate, M_m describes any polarization dependent losses in the steering mirrors and any other optics in the beam path, M_{wpi} is the ith waveplate, and $M_{x(y)}$ is the polarizing beam splitter. For convenience, we have defined $M_o = M_{wp1}M_{wp2}M_m$ and $M_i = M_m M_{wp2} M_{wp1}$. Except for M_s, the forms of these matrices are well known. M_s can be split into two matrices. The first represents the reflection from the substrate with no microwave field applied, while the second represents the electrooptically modulated (phase retarded) part of the reflected optical field. With a nonzero front surface reflectivity, the circuit substrate forms an etalon with a total reflection coefficient given by

$$r(\phi_0) = \frac{-r_f + r_b e^{-i\phi_0}}{1 - r_f r_b e^{-i\phi_0}} \tag{2}$$

where r_f and r_b are the effective reflection coefficients of the front and back surfaces of the GaAs substrate, and ϕ_0 is the roundtrip phase delay of the etalon. The total phase retardation experienced by the optical field within the substrate is proportional to $\int E_m \cdot dl$, where E_m is the applied microwave field and l is the path of the optical probing beam which may include multiple passes through the substrate. For a probe pulse which is long compared to the roundtrip optical transit time, the average number of passes is equal to the substrate etalon storage time divided by the roundtrip time. For a general etalon, this ratio is given by the phase derivative of the etalon reflection coefficient. Based on our earlier analysis [15], we can write M_s as

$$M_s = r(\phi_0)\left[I + \frac{\Gamma(\omega_m)}{2}\frac{\partial_{\phi_0} r(\phi_0)}{r(\phi_0)} S\right] \tag{3}$$

where I is the identity matrix, $\Gamma(\omega_m)$ is the electrooptically induced phase retardation (at a microwave frequency ω_m)

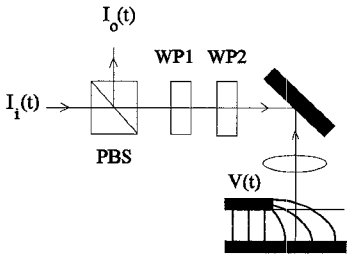

Fig. 1. A general schematic of the electrooptic sampling system for reflection-mode probing.

experienced by an optical field in one pass through the substrate, and S is a matrix whose value depends on the orientation of the GaAs substrate crystal axes. With the x- and y-axis representing the [110] and $[\bar{1}10]$ direction in GaAs, S can be written as

$$S = \begin{bmatrix} 1 & 0 \\ 0 & -1 \end{bmatrix}. \tag{4}$$

Assuming the input field is x-polarized, we can relate the input and output fields according to

$$E_o = (M_o M_s M_i)_{21} E_i \,. \tag{5}$$

The receiver signal (photo current) is proportional to the time averaged output intensity $\langle I_o \rangle \propto \langle E_o E_o^* \rangle$, where the angular brackets denote time averaging. Using (3) and expanding the time averaged output intensity to first order in the phase retardation Γ yields

$$\langle I_o \rangle = |r(\phi_0)|^2 \Bigg\{ |(M_o M_i)_{21}|^2 + 2\,\mathrm{Re} \cdot \left[\frac{\Gamma(\Delta\omega)}{2} \frac{\partial_{\phi_0} r(\phi_0)}{r(\phi_0)} \cdot (M_o S M_i)_{21} (M_o M_i)^*_{21} \right] \Bigg\} \langle I_i \rangle \tag{6}$$

where $\Delta\omega = \omega_m - N\omega_L$ is the intermediate frequency (IF) ($N\omega_L$ is the Nth harmonic of the laser pulse spectrum), and we have assumed that the average input intensity and the intensity in the Nth pulse train harmonic are the same ($\langle I_i \rangle$). The first term of (6) represents the receiver dc signal, while the second term represents the receiver IF signal. If we write $r = |r| \exp(-i\Phi)$, such that

$$\frac{\partial_{\phi_0} r(\phi_0)}{r(\phi_0)} = \partial_{\phi_0} \ln|r(\phi_0)| - i\partial_{\phi_0}\Phi(\phi_0)\,, \tag{7}$$

we see that there are generally two contributions to the IF signal. These two terms have different dependencies on the substrate parameters. The last term in (7) gives rise to the wanted polarization rotation modulation, while the first term results in a direct amplitude modulation (AM) due to the time varying etalon reflection coefficient. Depending on the substrate parameters and the polarization state of the incident probe beam, either of these two terms can dominate [15]. Fig. 2 shows the reflectivity, together with each of the two terms on the right-hand side of (7) times $|r|^2$, as a function of substrate thickness, parameterized by the backside reflectivity. Due to the sign change in the AM term at a roundtrip phase of o, the total IF signal is, in general, an asymmetric function of the substrate thickness. There is no way to separate the two IF signal contributions in the receiver. However, if there are no polarization dependent losses ($M_m = I$, we neglect any constant losses), the matrix $M_o S M_i$ is unitary, and it can be shown that $(M_o S M_i)_{21}(M_o S M_i)^*_{21}$ is purely imaginary. Therefore, the IF signal is proportional to $\partial_{\phi_0}\Phi$ only. Thus, any sampling system which is described by a unitary Jones matrix (apart from an overall constant) will show no direct AM. Conversely, to observe the direct AM term, the sampling head Jones matrix has to be nonunitary.

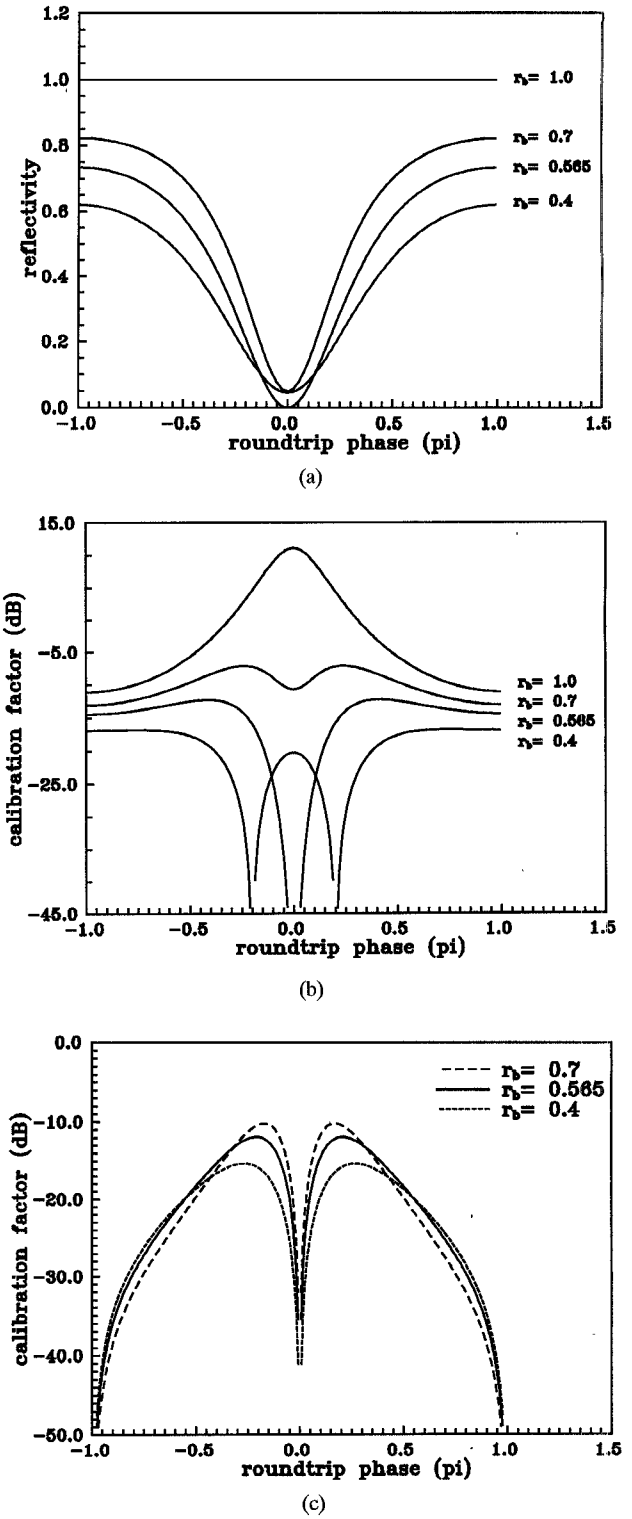

Fig. 2. Theoretical curves for (a) the substrate etalon reflectivity $|r(\phi_0)|^2$ and the IF signal proportionality factors, (b) $|r(\phi_0)|^2 \partial_{\phi_0}\Phi(\phi_0)$, and (c) $|r(\phi_0)|^2 \partial_{\phi_0} \ln|r(\phi_0)|$. $r_f = 0.565$, $r_b = 1.0$, 0.7, 0.565, and 0.4.

Because direct AM complicates signal interpretation, it is generally best to avoid polarization dependent losses in the sampling head. Our initial setup used five dielectric coated aluminum mirrors, and showed a 20% difference in loss for the

two polarization eigenstates. Replacing the aluminum mirrors with bare gold mirrors removed the unwanted polarization dependent loss. With the gold mirrors, the Jones matrix of the system could safely be treated as unitary, except for an overall loss constant. In this case, the most general form of the receiver signal can be expressed as

$$\langle I_o \rangle = |r(\phi_0)|^2 \left[I^o_{dc} + \partial_{\phi_0} \Phi(\phi_0) I^o_{if} \right] \tag{8}$$

where I^o_{dc} and I^o_{if} follow from (6). I^o_{dc} and I^o_{if} do not depend on the substrate parameters, and therefore represent the dc and IF receiver signal in the ideal case, in which there is no reflection from the front surface of the etalon and complete reflection from the back ($r = 1$ and $\partial_{\phi_0}\Phi = 1$); their values are only determined by the orientation of the waveplates and the crystal axes, and the applied microwave field. In general $|r(\phi_0)|^2$ and $\partial_{\phi_0}\Phi(\phi_0)$, with ϕ_0 a function of position, are needed to de-embed the effects of the substrate variations.

B. The Substrate Etalon

When fabricating microwave circuits on crystal wafers, the substrate is usually lapped and polished down to the proper thickness before a ground plane is deposited. Both the lapping/polishing process and the metallization process affect the optical properties of the substrate. A schematic depiction of a typical GaAs substrate is shown in Fig. 3. The top surface (air/GaAs) is usually very smooth and can be approximated as a perfect optical interface with reflection coefficient $r_f = (n_{GaAs} - 1)/(n_{GaAs} + 1) \simeq 0.565$ ($n_{GaAs} \simeq 3.6$). On the back surface, a 200 Å Ti layer, used as a bonding layer between the GaAs substrate and the Au ground plane, has been included. The Ti bonding layer is very lossy. With an index of refraction $n_{Ti} \sim 3.0 - i3.7$ [16], it is nearly index matched to the GaAs substrate and a large fraction of the optical power is therefore coupled into the bonding layer. The large imaginary component of the refractive index then results in high absorption. A 200 Å Ti layer backed by an electroplated gold reflector ($n_{Au} \simeq 0.47 - i2.83$ [17]) results in a net back surface reflection coefficient of $r_b \sim 0.55 e^{i0.7\pi}$. This low effective reflectivity can be further reduced due to residual fine scale surface roughness.

A 0.3 μm grit was used in the final polishing step performed on the wafer used in our experiment. This left a significant residual fine scale surface roughness in the ground plane that had to be included in the model of the substrate etalon. Details of this model are presented in the Appendix.

Under the assumption that the correlation length of the surface corrugations is much less than the probe beam width, the average etalon reflectivity is given by [(23) of the Appendix]

$$\left\langle |r(\phi_0)|^2 \right\rangle_x = \frac{r_f^2 + r_b^2 - 2 r_f r_b r_r \cos\phi_0 - \frac{r_f^2 r_b^2 (2 - r_f^2 - r_b^2)}{1 - r_f^2 r_b^2}(1 - r_r^2)}{\left| 1 - r_f r_b r_r e^{i\phi_0} \right|^2} \tag{9}$$

where the angular brackets with subscript x denote a spatial average over the beam spot, and the reduced backside reflection coefficient due to the rms surface roughness is defined as $r_r \equiv \exp\{-\frac{1}{2}\langle \phi^2 \rangle_x\}$. The phase of r_b has been absorbed into ϕ_0. Noting that $|r|^2 \partial_{\phi_0}\Phi$ can be written as $-Im\{r^* \partial_{\phi_0} r\}$, the IF signal proportionality constant follows as [(24) of the Appendix]

$$\left\langle |r(\phi_0)|^2 \partial_{\phi_0}\Phi(\phi_0) \right\rangle = (1 - r_f^2) r_b \,\mathrm{Re} \cdot \left\{ e^{i\phi_0} \frac{-r_f r_r A + r_b e^{-i\phi_0} B}{\left(1 - r_f^2 r_b^2\right)^2 (1 - r_f r_b r_r e^{-i\phi_0})(1 - r_f r_b r_r e^{i\phi_0})^2} \right\} \tag{10}$$

where

$$A = \left(1 - r_f^2 r_b^2 r_r\right)^2 - (1 - r_r) 2 r_f^2 r_b^2 + \left(1 - r_r^2\right) r_f^2 r_b^4 \tag{11}$$

$$B = \left(1 - r_f^2 r_b^2 r_r\right)^2 + (1 - r_r) 2 r_f^2 r_b^2 r_r + \left(1 - r_r^2\right) r_f^2 . \tag{12}$$

As shown in Fig. 4(a), the phase uncertainty across the probe beam reduces the contrast of the dc signal. For very small surface roughness effects ($r_r \sim 1$) and the r_b not too close to r_f, the effect of the roughness is almost identical to a slightly reduced backside reflection coefficient (r_b). For the IF signal, shown in Fig. 4(b), the situation is different. In this case, for very small roughness effects, the effect is similar to an increase in the backside reflection coefficient. We note that both the dc and IF signal dependence on r_r are consistent with a convolution of the signals with $r_r = 1$ with a phase uncertainty function. In general, the surface roughness has to be treated as an independent parameter if it becomes a significant factor (i.e., if the data cannot be successfully de-embedded ignoring the roughness parameter). However, in the small roughness limit, one can avoid introducing this additional parameter, as we discuss in the next section.

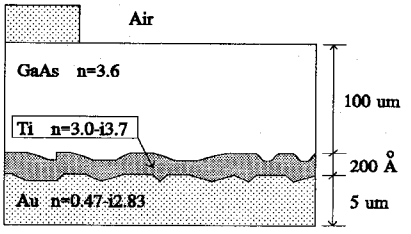

Fig. 3. Schematic diagram of GaAs substrate.

C. De-Embedding Procedure

It is evident from (9) and (10) that local variations in the substrate thickness, on scales both longer and shorter than the sampling beam diameter, can greatly affect raw electrooptic sampling measurements of the spatial variation of the microwave potential within a particular circuit. Accurate determination of the microwave potential therefore requires that a measurement of the local properties of the substrate etalon be used to de-embed the effect of substrate nonuniformities. In this sub-section, we will present a technique which uses the spatial variation of the dc receiver signal (which gives the average total effective reflectivity of the substrate) to compute a spatially varying correction factor. In Section IV, other possibilities will be discussed.

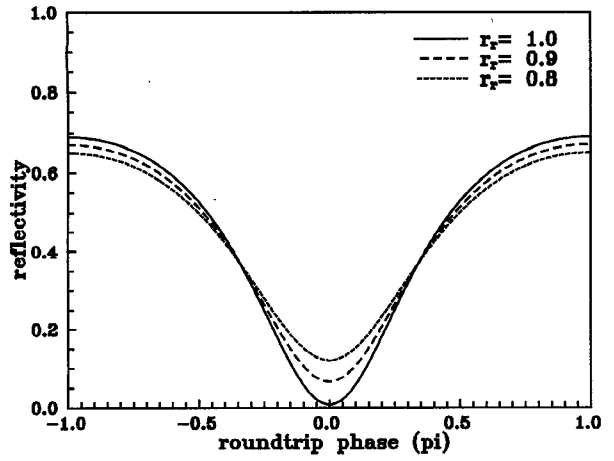

(a)

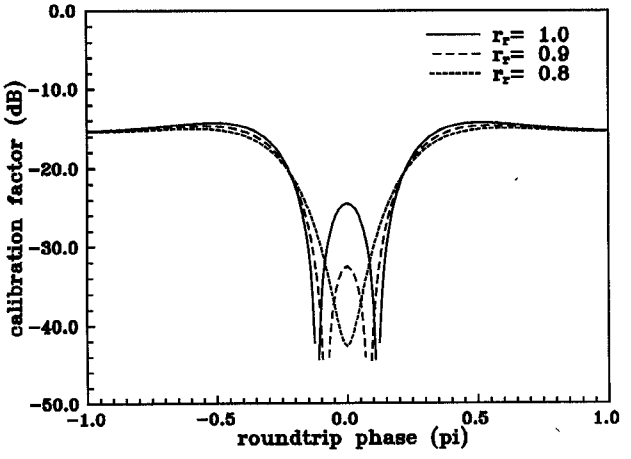

(b)

Fig. 4. Theoretical curves for (a) the average substrate etalon reflectivity $\langle |r(\phi_0)|^2 \rangle_x$, and (b) the IF signal proportionality factor $\langle |r(\phi_0)|^2 \partial_{\phi_0} \Phi(\phi_0) \rangle_x$ for various surface roughness parameters. $r_f = 0.565$, $r_b = 0.5$, and $r_r = 1.0, 0.9, 0.8$.

From (6) it follows that the dc receiver signal is directly proportional to the substrate etalon reflectivity. Inverting that equation, we can express the cosine of the local phase delay as

$$\cos[\phi_0(x)] = \frac{r_f^2 + r_b^2 - \frac{r_f^2 r_b^2 (2 - r_f^2 - r_b^2)}{1 - r_f^2 r_b^2}\left(1 - r_f^2\right) - s(x)\left(1 + r_f^2 r_b^2 r_r^2\right)}{2 r_f r_b r_r [1 - s(x)]} \tag{13}$$

where $s(x)$ is the normalized dc receiver signal

$$s(x) = R_{min} + (R_{max} + R_{min}) \frac{I(x) - I_{min}}{I_{max} + I_{min}}. \tag{14}$$

$I(x)$ is the measured dc receiver signal, $I_{min(max)}$ is the measured minimum (maximum) dc signal, and $R_{min(max)}$ is the theoretical minimum (maximum) substrate etalon reflectivity for a given r_f, r_b, and r_r. It is assumed that one has measured over a large enough area that the roundtrip phase has sampled the full range from 0 to π. Once the local phase delay is known, the IF receiver signal proportionality factor can be calculated as

$$\left\langle |r(\phi_0)|^2 \partial_{\phi_0} \Phi(\phi_0) \right\rangle_x = \frac{\left(1 - r_f^2\right) r_b}{\left(1 - r_f^2 r_b^2\right)^2} \cdot \frac{r_b\left(B + A r_f^2 r_r^2\right) - r_f r_r \left(A + B r_b^2\right) \cos[\phi_0(x)]}{\left\{1 + r_f^2 r_b^2 r_r^2 - 2 r_f r_b r_r \cos[\phi_0(x)]\right\}^2}. \tag{15}$$

The de-embedding algorithm normalizes each spatial measurement according to (14), and uses (13) and (15) to calculate the proper local correction factor. The corrected IF data (proportional to the microwave potential) are then calculated according to

$$I_{cor} = \frac{I_{meas,IF}}{\left\langle |r(\phi_0)|^2 \partial_{\phi_0} \Phi(\phi_0) \right\rangle_x}. \tag{16}$$

In general, r_f, r_b, and r_r are unknown, and they will vary from circuit to circuit, depending on the processing used in fabricating the ground plane. However, for a well-controlled fabrication process, it is reasonable to assume that these parameters are constant across a particular circuit. Furthermore, for a clean front surface, one can safely assume that r_f is given by the Fresnel reflection from an air/GaAs dielectric interface ($r_f = 0.565$). The other two parameters, r_b and r_r, can be determined from a calibration standard with a known field distribution and a curve fitting technique. For example, the field amplitude along a well-terminated transmission line is known to be constant. Therefore, a single scan electrooptic sampling measurement can be made along such a calibration standard which has been included on the substrate to be tested. Then, by assuming $r_f = 0.565$ (or some other appropriate value) and assigning reasonable values to r_b and r_r, the data scan can be "corrected" according to the procedure discussed above. The parameters can then be adjusted to best match the inverted data to the known field distribution. For the case of a constant field, this can easily be done by minimizing the variance of the corrected data.

If the surface roughness is a weak effect, only one unknown parameter (r_b) is needed. In this case, satisfactory IF signal correction (small variance) can be achieved by choosing an r_b value resulting in a theoretical dc signal contrast higher than the contrast in the measured dc signal. As shown in the previous section, on the IF data, a very small roughness effect is similar to a slight increase in r_b. Therefore, a good correction of the IF data can be obtained by using a value of r_b that results in a higher contrast in the theoretical dc signal than in the measured dc data. The only significant error in setting $r_r = 1$ in this case occurs at isolated points close to the zero crossings of the IF correction factor. To avoid that, the errors close to these zero crossings affect the fitting, all points whose correction exceeded a certain threshold were dropped from the variance calculation.

III. Measurements

The effectiveness of the de-embedding procedure proposed in the previous section was tested with electrooptic sampling measurements made along microstrip transmission lines fabricated on a GaAs wafer. The wafer was lapped down to a 100 μm thickness and polished with a series of grits, the final size of which was 0.3 μm. A 200 Å evaporated Ti layer was used as an adhesive layer for the 5 μm electroplated gold ground plane. A standard electrooptic sampling setup was used for normal incidence reflection-mode probing of GaAs circuits [14], [15]. As discussed in Section II-B, care was taken to avoid any polarization dependent losses in the sampling system by using uncoated Au mirrors. A modelocked Nd: YAG laser was used to produce 90 ps pulses with nearly Gaussian shape. The average optical power incident on the circuit was kept below 20 mW. The probe beam was focused to a spot size of about 10 μm using a 5× microscope objective. To allow for very accurate spatial scans, a wafer probe station was mounted on a stepper motor controlled x-y platform, and a step size of 5 μm (much larger than the 0.1 μm resolution of the stepper motor stages) on a square grid was used. A video camera and a TV monitor were used to precisely position the probe beam at the starting position. The experiment was controlled from a computer to automate the measurement process.

To fix the unknown global parameter r_b (we set $r_r = 1$ consistent with small roughness effects) for the wafer under consideration, a single spatial scan along a through-line of an on-wafer microstrip TRL calibration standard was taken. Using $r_f = 0.565$, r_b was obtained by minimizing the variance of the corrected data as described in the previous section. This process is illustrated in Fig. 5, where we show the variance of the corrected IF data as a function r_b [Fig. 5 (a)] and the spatial variation of the corrected IF data [Fig. 5 (b)] for three different values of r_b. Compliant with the discussion in the previous section, all points whose correction was larger than 30 dB were dropped from the variance calculation. The value of r_b determined by the minimum variance of the corrected IF data ($r_b = 0.43$) is slightly higher than the value corresponding to the measured contrast ($r_b = 0.41$), even though the correction of the IF data is very good, indicating the surface roughness scattering is only a weak effect.

A 2D electrooptic sampling measurement was then made right next to the terminated calibration strip as shown in Fig. 6. The raw data are shown in Fig. 7. By applying the de-embedding procedure described in Section II-C, we obtained the corrected microwave potential shown in Fig. 8. Clearly, there is a significant improvement in the de-embedded data as compared to the raw IF data [Fig. 7 (a)]. The residual spikes along the locations of the minimums of the raw data are due to the zero signal-to-noise ratio at these points (and the fact that we set $r_r = 1$) resulting in an overcompensation. Physically, the potential cannot vary this fast spatially, so with proper processing these points can be taken out of the data without loss of information. The resulting 2D potential, apart from the spikes, is equal to what one would expect on a straight microstrip transmission line.

A more interesting case is provided by the open-end microstrip line shown in Fig. 9. The raw data as measured

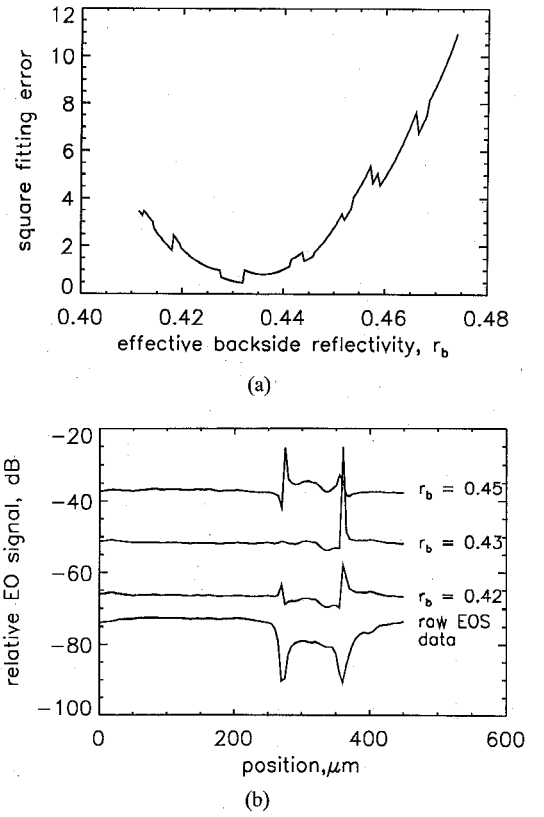

Fig. 5. 9a) Variance of the corrected IF data as a function of backside reflectivity, and (b) the spatial variation of the corrected IF data. The corrected IF data for $r_b = 0.43$ and 0.42 are displaced by −15 dB and −30 dB for clarity.

at 5 GHz is shown in Fig. 10. After using the above de-embedding procedure, the measurements were enhanced with a simple postcorrection processing procedure. All points whose correction exceeded a certain threshold (30 dB in this case), were replaced by an average of two surrounding points. The entire data set was then smoothed with a 10 point (50 μm) square median filter, and the result is shown in Fig. 11.

IV. Discussion

These initial experiments demonstrate the validity of the models presented, and the feasibility of the de-embedding process. The most serious problem is the vanishing signal-to-noise ratio at the spatial locations where the optical beam sees a resonant substrate etalon. The correction factors near these points are quire large (>20 dB) and are very sensitive to the substrate parameters. The procedure presented here can have

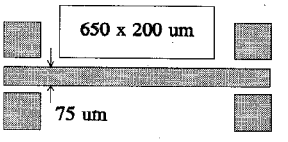

Fig. 6. Layout of the microstrip through-line. The microwave potential was probed in the 200 × 650 μm^2 area. A measurement grid of 40 × 130 points was used.

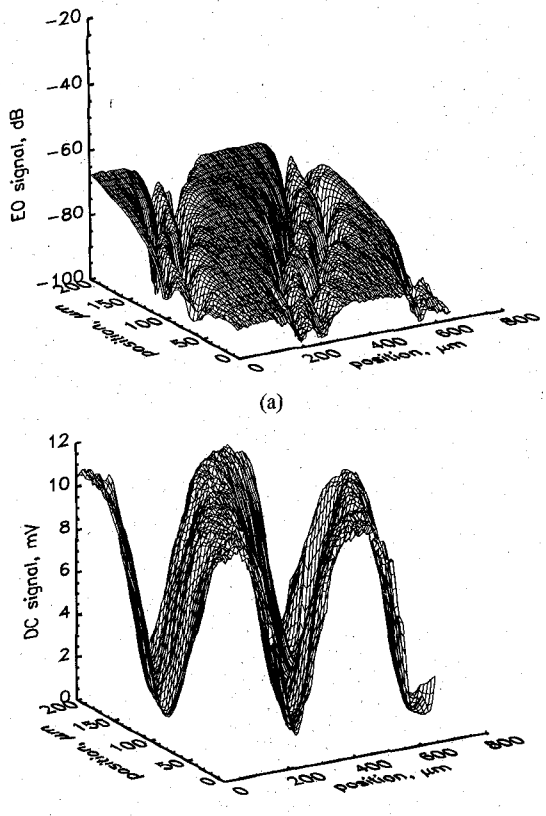

Fig. 7. Measured variation of (a) the IF signal and (b) the dc signal next to the microstrip through-line shown in Fig. 6.

large errors at these isolated points (lines). However, because the potential cannot vary on the small length scale associated with these uncorrectable points, an image processing algorithm has been used to take advantage of this and to filter these points out of the data set. As demonstrated in Fig. 11, a

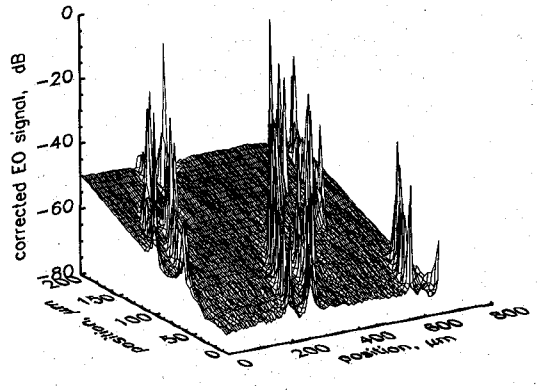

Fig. 8. Corrected microwave potential distribution next to the microstrip through-line shown in Fig. 6.

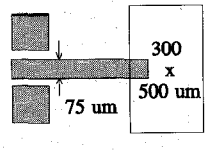

Fig. 9. Layout of the microstrip open-end. The potential was probed in the $500 \times 300\ \mu m^2$ area. A measurement grid of 100×60 points was used.

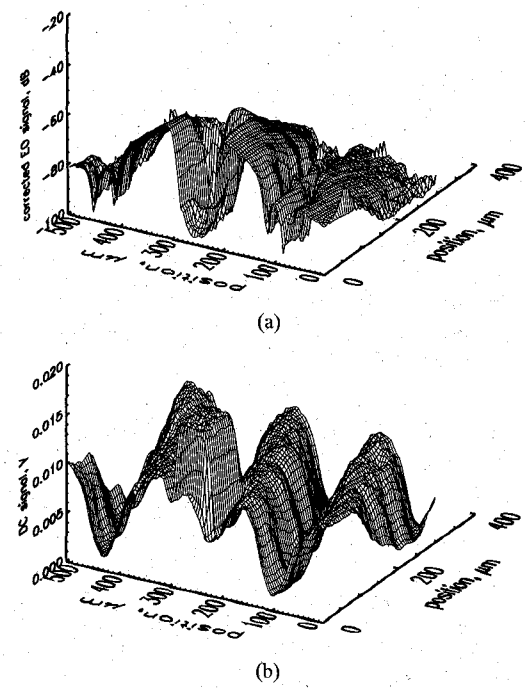

Fig. 10. Measured variation of (a) the IF signal, and (b) the dc signal around the microstrip open-end shown in Fig. 9.

median filtering seems to work well without a significant loss of structure in the data. Spatial frequency domain filtering could also be used to remove noise at the frequencies near the inverse pixel spacing.

There are also a number of ways in which the measurement procedure itself can be modified to overcome the problem of signal deterioration. The first, and conceptually simplest, is to use probe pulses much shorter than the optical transit time of the substrate. In this case, the IF signal is only weakly influenced by the variations in the substrate thickness [15]. However, advanced (expensive) laser systems are needed to generate the ultrashort (typically subpicosecond) pulses required, and many practical applications do not need the high temporal resolution afforded by such pulses. It is also possible to use chirped (broadband) pulses whose temporal coherence time is less than the substrate roundtrip time, so as to reduce interference effects. Gain switched semiconductor

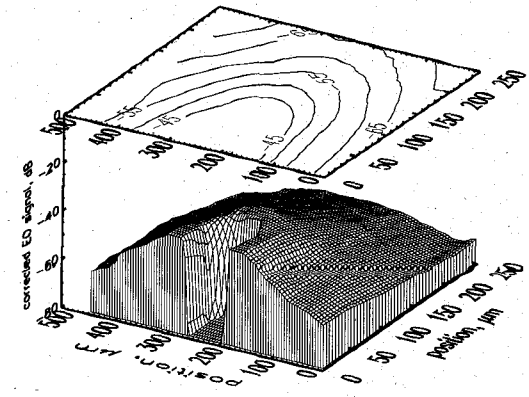

Fig. 11. Corrected microwave potential distribution around the microstrip open-end shown in Fig. 9.

lasers typically do have a very significant chirp, but it is not enough to eliminate the interference completely. This then leads to another parameter (temporal coherence time) in the de-embedding algorithm, and therefore complicates data processing.

For a practical, small, and economical system, one elegant solution would be to use two laser wavelengths separated by approximately one-half free spectral range of the substrate etalon (typically on the order of one nanometer). Semiconductor laser diodes can be temperature/injection-current tuned to lock two lasers at such a wavelength separation by deriving a feedback signal from the transmission through a tunable etalon (e.g., an angle tuned air-spaced etalon). The two probe wavelengths would be close enough together that the optical properties of the sampling system would be the same, and the beams from the two lasers could be combined into a fiber and launched into the sampling system. When one wavelength experiences a resonance, the other would be off resonance, thereby maintaining a high signal-to-noise ratio. The measurement data produced by such a system could then be processed using a straightforward modification of the technique presented here.

V. Conclusion

We have presented a technique for measuring the two-dimensional microwave potential distribution on GaAs microwave circuits. The technique is based on the direct electrooptic sampling technique and a de-embedding procedure based on a theoretical model of the electrooptic sampling system and circuit substrate. The model relates the measured dc and IF signals to the applied microwave signal and several unknown substrate etalon parameters, the substrate optical roundtrip phase, the front and back surface reflectivities, and a surface roughness parameter. The front and back surface reflectivities and the surface roughness parameter are determined from a single scan electrooptic sampling measurement along a calibration standard (with known field distribution) and a curve fitting technique. The microwave potential is determined from the measured electrooptic signal (IF signal) by deducing the local optical roundtrip phase from the locally measured reflectivity (dc signal). The microwave potential is then calculated from the measured electrooptic signal using a model for the electrooptic sampling system containing the global etalon parameters (r_f, r_b, and r_r) and the local roundtrip phase $[\phi_0(x)]$.

The 2D microwave potential mapping system, with the associated de-embedding algorithm, can provide accurate high-resolution "images" of the potential near microwave devices. Applying the technique to 50 Ω microstrip lines on GaAs substrates, we demonstrated 2D mapping with 50 dB dynamic range and 10 μm spatial resolution. The measurement system and de-embedding procedure are readily computerized and automated to implement an automated 2D microwave potential measurement system. Furthermore, by using diode lasers or diode pumped solid state lasers, the cost and complexity of the required equipment can be drastically reduced.

Appendix

A. An Etalon with Rough Surfaces

In this appendix, we present an analysis of the effective reflection coefficient and electrooptic sampling signal expected from measurements performed on a circuit with mild surface roughness. The analysis is based on a scalar Fresnel–Kirchhoff diffraction integral [18], [19]. For a reasonably smooth surface (locally flat, i.e., composed of irregularities with small curvature), we can neglect the depolarization that will inevitably occur with reflection from a rough surface [19]. The depolarization is significant only for large scattering angles, and this light is not captured by the detector in the electrooptic sampling system.

The Kirchhoff diffraction integral for the specular field produced by the reflection of a plane wave from a slightly rough surface A, at a distance $r >> \sqrt{A}$, can be written as

$$E_r(x,y,z) = \int\int_A dx'\,dy' \frac{1}{i2\lambda r} \cdot \exp\{ik[r_0 + 2\zeta(x',y')]\} E_i(x',y') \qquad (17)$$

where r is the distance from a point on the surface $[x', y', \zeta(x', y')]$ to the observation point (x, y, z), and r_0 is the distance from the observation point to a point on the mean surface plane $(x', y', 0)$. A point on the rough surface is defined by its position (x', y') and height (in the z-direction) $\zeta(x', y')$. If $r >> \lambda$, then it is possible to approximate $r \simeq r_0$ so that the only dependence on the surface roughness $\zeta(x', y')$ appears in the exponential term. In the Fresnel approximation, (17) looks like diffraction from a random phase grating. Thus, the reflected field is proportional to the Fourier transform of $\exp[i2k\zeta(x', y')]$ times a quadratic phase factor. We can therefore write

$$E_r(x,y,z) \simeq e^{ikz} e^{i\phi(x,y)} E_i(x,y) \qquad (18)$$

where $\phi(x, y)$ is a zero mean random phase factor, and we have neglected the diffraction of E_i. The average value of the reflected intensity may be computed by using the appropriate probability density function $p(\zeta)$. The resulting average reflectivity cannot, however, be used in the standard formula for the etalon reflectivity, because the total reflectivity is determined by the interference of the partial waves whose phases results from an accumulation of surface scattering at all previous round trips. However, each reflection producing a partial wave can be treated as above, and be represented by an equation like (18).

In order to model a wafer which has been well polished only on one side, we consider an etalon with one smooth and one rough surface. The total reflection coefficient from the smooth surface can be expressed as the sum of an infinite number of partial waves produced by reflections from the two surfaces. Using (18), this can be written as

$$E_r(x) = \left\{ -r_f + \left(1 - r_f^2\right) r_b e^{i\phi_0} \right.$$

$$\cdot \sum_{n=0}^{\infty} \left(r_f r_b e^{i\phi_0}\right)^n \exp\left[i \sum_{j=1}^{n+1} \phi_j(\boldsymbol{x})\right] \Bigg\} E_i(\boldsymbol{x}) \tag{19}$$

where $\boldsymbol{x}$ is the transverse position vector, $E_{r(i)}(\boldsymbol{x})$ is the spatial varying reflected (incident) electric field, and $\phi_j(\boldsymbol{x})$ is the phase contribution due to surface roughness encountered during roundtrip j through the etalon. $\phi_j(\boldsymbol{x})$ is a complicated function of the surface properties and, at best, only the statistical properties of the surface will be known. Therefore, we can evaluate the reflected field only in a statistical sense. $\phi(\boldsymbol{x})$ is effected by the surface roughness scattering at all previous roundtrips. However, for an etalon much thicker than the optical wavelength λ, even small angle scattering causes the resulting spatial translation after one roundtrip to be large compared to the correlation length of the surface roughness (which has been assumed to be quite short). Therefore, it is safe to approximate the correlation functions as

$$\langle \phi_i(\boldsymbol{x}) \phi_j(\boldsymbol{x}') \rangle_x = \delta_{ij} \langle \phi_j(\boldsymbol{x}) \phi_j(\boldsymbol{x}') \rangle_x \tag{20}$$

where the angle brackets indicate a spatial average. Furthermore, we assume that the correlation length of the surface corrugations is much less than the probe beam diameter such that we can use the approximation

$$\langle \phi_j(\boldsymbol{x}) \phi_j(\boldsymbol{x}') \rangle_x \simeq \langle \phi^2 \rangle_x \delta(\boldsymbol{x} - \boldsymbol{x}') \tag{21}$$

where $\langle \phi^2 \rangle_x$ is the rms phase deviation which is assumed to be independent of j. It is quite reasonable to assume Gaussian statistics for the surface corrugations such that we can write

$$\left\langle e^{i[\phi_k(\boldsymbol{x}) - \phi_l(\boldsymbol{x}')]} \right\rangle_x = e^{\frac{1}{2}\delta_{kl} \langle \phi_l(\boldsymbol{x}) \phi_l(\boldsymbol{x}') \rangle_x}. \tag{22}$$

With the above assumptions, we can sum the double series for the reflected intensity and find (23). As shown in Section II, the IF receiver signal is proportional to $\langle E_r^* \partial_{\phi_0} E_r \rangle_x$. Again, we can sum the double series and express this proportionality constant as shown in (23) and (24) at the bottom of the page, where

$$A = \left(1 - r_f^2 r_b^2 e^{-\frac{1}{2}\langle \phi^2 \rangle_x}\right)^2 - \left(1 - e^{-\frac{1}{2}\langle \phi^2 \rangle_x}\right) 2 r_f^2 r_b^2 + \left(1 - e^{-\langle \phi^2 \rangle_x}\right) r_f^2 r_b^4 \tag{25}$$

$$B = \left(1 - r_f^2 r_b^2 e^{-\frac{1}{2}\langle \phi^2 \rangle_x}\right)^2 + \left(1 - e^{-\frac{1}{2}\langle \phi^2 \rangle_x}\right) 2 r_f^2 r_b^2 e^{-\frac{1}{2}\langle \phi^2 \rangle_x} - \left(1 - e^{-\langle \phi^2 \rangle_x}\right) r_f^2 . \tag{26}$$

Clearly, as $\langle \phi^2 \rangle_x \to 0$ (i.e., when there is no surface roughness), (23) reduces to the previous expression for the etalon reflectivity, and (24) reduces to the previous expression for the etalon effective storage time $|r|^2 \partial_{\phi_0} r / r$ [15].

ACKNOWLEDGMENT

The authors would like to thank T. Nichols for fabricating the microstrip test structures used in the experiments.

REFERENCES

[1] H. Hasegawa, M. Furukawa, and H. Yanai, "Measurements on high-frequency transmission characteristics of metallization patterns in monolithic i.c.s'," *Electron. Commun. Japan,* vol. 54-B, pp. 52–60, 1971.

[2] P. H. Ladbrooke, "A novel standing-wave indicator in microstrip," *Radio Electron. Engineer,* vol. 44, pp. 273–280, 1974.

[3] K. Solbach, "Electric probe measurements on dielectric image lines in the frequency range of 26–90 GHz," *IEEE Trans. Microwave Theory Tech.,* vol. MTT-26, pp. 755–758, 1978.

[4] S. E. Schwarz and C. W. Turner, "Measurement technique for planar high-frequency circuits," *IEEE Trans. Microwave Theory Tech.,* vol. MTT-344, pp. 463–467, 1986.

[5] S. S. Osofsky and S. E. Schwarz, "A non-contacting probe for measurements on high-frequency planar circuits," in *1989 IEEE Int. Microwave Symp. Dig.,* 1989, pp. 823–825.

[6] S. Sridhar, "Experimental observation of scarred eigenfunctions of chaotic microwave cavities," *Phys. Rev. Lett.,* vol. 67, pp. 785–788, 1991.

[7] S. L. McCall, P. M. Platzman, R. Dalichaouch, D. Smith, and S. Schultz, "Microwave propagation in two-dimensional dielectric lattices," *Phys. Rev. Lett.,* vol. 67, pp. 2017–2020, 1991.

[8] D. G. Stearns, "Electro-optic sampling of ultrashort high voltage pulses," *J. Appl. Phys.,* vol. 65, pp. 1308–1315, 1989.

[9] L. E. Kingsley and W. R. Donaldson, "Electrooptic imaging of surface electric fields in high-power photoconductive switches," *IEEE Trans. Electron Devices,* vol. 37, pp. 2449–2458, 1990.

[10] W. R. Donaldson, L. Kinglsey, M. Weiner, A. Kim, and R. Zeto, "Electro-optic imaging of the internal fields in a GaAs photoconductive switch," *J. Appl. Phys.,* vol. 68, pp. 6453–6457, 1990.

[11] G. Plows, "Electron-beam probing," in *Measurement of High-Speed Signals in Solid State Devices,* R. B. Marcus, Ed. New York: Academic, 1990; pp. 335–382.

[12] A. M. Weiner and R. B. Marcus, "Photoemissive probing," in *Measurement of High-Speed Signals in Solid State Devices,* R. B. Marcus, Ed. New York: Academic, 1990, pp. 383–420.

$$\langle E_r E_r^* \rangle_x = \frac{r_f^2 + r_b^2 - 2 r_f r_b e^{-\frac{1}{2}\langle \phi^2 \rangle_x} \cos\phi_0 - \frac{r_f^2 r_b^2 \left(2 - r_f^2 - r_b^2\right)}{1 - r_f^2 r_b^2} \left(1 - e^{-\langle \phi^2 \rangle_x}\right)}{\left|1 - r_f r_b e^{-\frac{1}{2}\langle \phi^2 \rangle_x} e^{i\phi_0}\right|^2} \left\langle |E_i|^2 \right\rangle . \tag{23}$$

$$\langle E_r^* \partial_{\phi_0} E_r \rangle_x = -i\left(1 - r_f^2\right) r_b \left\{ \frac{e^{i\phi_0} \left(-r_f e^{-\frac{1}{2}\langle \phi^2 \rangle_x} A + r_b e^{-i\phi_0} B\right)}{\left(1 - r_f^2 r_b^2\right)^2 \left(1 - r_f r_b e^{-\frac{1}{2}\langle \phi^2 \rangle_x} e^{-i\phi_0}\right) \left(1 - r_f r_b e^{-\frac{1}{2}\langle \phi^2 \rangle_x} e^{i\phi_0}\right)^2} \right\} \left\langle |E_i|^2 \right\rangle \tag{24}$$

[13] H. Bergner, T. Damm, U. Stamm, M. Müller, K.-P. Stolberg, and H. Seidel, "Investigation of internal signal propagation of an integrated circuit with high temporal resolution," in *Ultrafast Phenomena in Spectroscopy,* E. Klose and B. Wilhelmi, Eds. Berlin: Springer-Verlag, 1990, pp. 121–124.
[14] K. J. Weingarten, M. J. W. Rodwell, and D. M. Bloom, "Picosecond optical sampling of GaAs integrated circuits," *IEEE J. Quantum Electron.,* vol. QE-24, pp. 198–220, 1988.
[15] D. R. Hjelme and A. R. Mickelson, "Voltage calibration of the direct electrooptic sampling technique," *IEEE Trans. Microwave Theory Tech.,* vol. MTT-40, pp. 1941–1950, 1992.
[16] T. Smith, "Optical constants of clean Titanium and Tungsten surfaces as function of temperature," *J. Opt. Soc. Amer.,* vol. 62, pp. 774–780, 1972.
[17] M. Born and E. Wolf, *Principles of Optics,* 6th ed. Oxford: Pergamon, 1980.
[18] H. Davies, "The reflection of electromagnetic waves from a rough surface," in *Proc. IEE,* vol. 101, pp. 209–214, 1954.
[19] P. Beckmann and A. Spizzichino, *The Scattering of Electromagnetic Waves From Rough Surfaces.* New York: Pergamon, 1963.

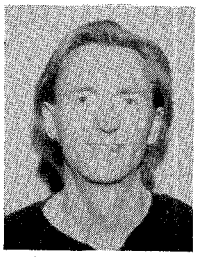

Dag Roar Hjelme was born in Valldal, Norway, on March 25, 1959. He received the M.S. degree in electrical engineering from the Norwegian Institute of Technology, Trondheim, Norway, in 1982, and the Ph.D. degree in electrical engineering from the University of Colorado, Boulder, in 1988.

From 1983 to 1984 he was with the Norwegian Institute of Technology, Division of Physical Electronics, working on fiber optics and integrated optics. He is currently a Postdoctoral Research Associate with the Department of Electrical Engineering, University of Colorado. His current research interests include the dynamic and spectral properties of semiconductor lasers, microwave optics, and optoelectronics.

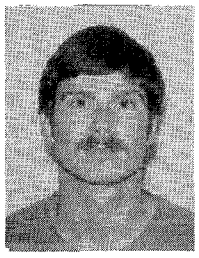

Michael John Yadlowsky was born in Silver Spring, MD, on June 21, 1965. He received the B.S. degree in electrical engineering from the University of Virginia in 1987 and the M.S. and Ph.D. degrees in electrical engineering from the University of Colorado at Boulder in 1990 and 1992, respectively.

He is currently a Research Associate with the Cooperative Institute for Research in Environmental Sciences (CIRES) and the Department of Electrical and Computer Engineering/DDx Incorporated. His current research interests include lidar, electromagnetic propagation, and biomedical applications of optics, particularly optical immunoassays.

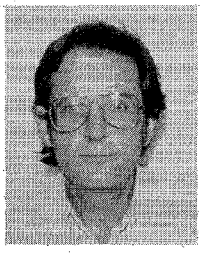

Alan Rolf Mickelson was born in Westport, CT, on May 2, 1950. He received the B.S.E.E. degree from the University of Texas, El Paso, in 1973, and the M.S. and Ph.D. degrees from the California Institute of Technology, Pasadena, in 1974 and 1978, respectively.

Following a postdoctoral period at Caltech in 1980, he joined the Electronics Research Laboratory of the Norwegian Institute of Technology, Trondheim, Norway, at first as an NTNF Postdoctoral Fellow, and later as a staff scientist. His research in Norway primarily concerned characterization of optical fibers and fiber compatible components and devices. In 1984 he joined the Department of Electrical and Computer Engineering at the University of Colorado, Boulder, where he became an Associate Professor in 1986. His research presently involves semiconductor laser characterization, integrated optic device fabrication and characterization, and fiber system characterization.